## Proper Thermal Equilibration of Simulations with Drude Polarizable Models : Temperature Grouped Dual-Nosé-Hoover Thermostat

Chang Yun Son, †,‡ Jesse G. McDaniel, †,¶ Qiang Cui, †,§ and Arun Yethiraj\*,†

Department of Chemistry and Theoretical Chemistry Institute, University of Wisconsin-Madison, 1101

University Avenue, Madison, WI 53706, Present address: Division of Chemistry and Chemical

Engineering, California Institute of Technology, Pasadena, CA 91125, Present address: School of

Chemistry and Biochemistry, Georgia Institute of Technology, Atlanta, GA 30332, and Present address:

Department of Chemistry, Department of Biomedical Engineering and Department of Physics, Boston

University, 590 Commonwealth Avenue, Boston, MA 02215

Received November 19, 2019; E-mail: yethiraj@wisc.edu

Abstract: An explicit treatment of electronic polarization is critically important to accurate simulations of highly charged or interfacial systems. Compared to the iterative self consistent field (SCF) scheme, extended Lagrangian approaches are computationally more efficient for simulations that employ a polarizable force field. However, an appropriate thermostat must be chosen to minimize heat flow and ensure an equipartition of kinetic energy among all unconstrained system degrees of freedom. Here we investigate the effects of different thermostats on the simulation of condensed phase systems with the Drude polarizable force field using several examples that include water, NaCl/water, acetone and an ionic liquid (IL)  $BMIM^+/BF_4^-$ . We show that conventional dual-temperature thermostat schemes often suffer from violations of equipartitioning and adiabatic electronic state, leading to considerable errors in both static and dynamic properties. Heat flow from the real degrees of freedom to the Drude degrees of freedom leads to a steady temperature gradient and puts the system at an incorrect effective temperature. Systems with high-frequency internal degrees of freedom such as planar improper dihedrals or C-H bond stretches are most vulnerable; this issue has been largely overlooked in the literature due to the primary focus on simulations of rigid water molecules. We present a new temperature-grouped dual Nosé-Hoover thermostat, where the molecular center of mass translations are assigned to a temperature group separated from the rest degrees of freedom. We demonstrate that this scheme predicts correct static and dynamic properties for all the systems tested here, regardless of the thermostat coupling strength. This new thermostat has been implemented into the GPU-accelerated OpenMM simulation package and maintains a significant speed up relative to the SCF scheme.

Molecular dynamics (MD) simulations have become an indispensable tool for the analysis of condensed phases, including biological systems and energy materials. For systems with a high ionic or dipolar composition, electrostatic interactions and electronic polarization play a central role in determining the structural and dynamic properties. While an implicit treatment of electronic polarization has proven successful for the description of many neat liquids, it is increasingly recognized that an explicit treatment of electronic

polarization is required for the prediction of many properties of complex fluids, such as dynamics and phase behaviors of ionic liquids, <sup>2–5</sup> ion distribution at the air/water interface, <sup>6</sup> ion correlation in organic electrolytes, <sup>7</sup> and the temperature dependence of a cooperative protein folding process. <sup>8</sup>

Molecular simulations with a polarizable force field require both a model potential function (e.g., with Drude oscillators or atomic polarizabilities) and a method for determining the magnitude and orientation of the induced dipoles. 1,9-12 For the latter, extended Lagrangian schemes are increasingly utilized due to their computational efficiency over the self consistent field (SCF) scheme, and they have recently been implemented in most major MD software packages. 13-17 These schemes utilize two-temperature thermostats (dualthermostat) to keep the electronic degrees of freedom (DOF) at a very low temperature compared to the actual system temperature.  $^1$  However, such an ansatz intrinsically creates heat flow from the system to the Drude DOF, which, if significant, leads to the violation of kinetic energy equipartitioning and thus artifacts in computational results. 18 Appropriate control of adiabatic conditions of electronic state is also of central importance in Car-Parrinello-like ab initio molecular dynamics simulations using extended Lagrangian scheme. 19

A systematic analysis of thermostat schemes in polarizable force field simulations is thus warranted. Indeed, even for simulations with non-polarizable force fields, several recent studies  $^{20-23}$  highlighted potential subtleties. Basconi and Shirts  $^{23}$  discussed the artifact of thermostats that randomize the velocities, with which the translational motions of molecules are systematically retarded with a stronger coupling to the heat bath. On the other hand, thermostats that rescale system velocities may fail to evenly distribute the kinetic energy among different DOF, resulting in artifacts such as the 'flying ice cube' or 'hot solvent/cold solute'. <sup>20</sup> Subtle differences in the partitioning of kinetic energy can also lead to qualitatively different predictions of bulk properties for water.  $^{24-26}$ 

In the present work, we systematically investigate the effects of different thermostat schemes in polarizable simulations employing the Drude oscillator model. We focus on two common dual-thermostat schemes, the velocity randomizing dual-Langevin  $^{14}$  (dual-LV) thermostat and the velocity rescaling dual-Nosé-Hoover  $^{13}$  (dual-NH) thermostat. For each thermostat, a wide range of thermostat parameters  $\tau$  and  $\tau^*$  are tested, which represents coupling time to the heat bath for the real and Drude DOF (see Methods), respectively. By comparing simulations for a variety of liquids,

 $<sup>^\</sup>dagger {\it University}$  of Wisconsin-Madison

<sup>&</sup>lt;sup>‡</sup>Caltech

 $<sup>\</sup>P_{\text{Georgia}}$ 

 $<sup>\</sup>S{\,{\rm BU}}$ 

which include water, NaCl/water, acetone, and BMIM<sup>+</sup>BF<sub>4</sub> ionic liquid, we highlight that achieving equipartitioning within a dual-thermostat ansatz is challenging and requires care for systems with high-frequency intramolecular modes. This is because the high frequency modes have a larger overlap with the power spectrum of the Drude oscillators, leading to significant heat flow from the high temperature to low temperature bath. Applying a velocity randomizing thermostat with strong friction couplings  $(\tau, \tau^* < 1ps)$  is thus necessary for maintaining a rigorous thermal equipartition, but this can significantly perturb the system dynamics (vide infra).

In cases where high frequency modes are either unphysical or unimportant, it may be practically advantageous to partially relax the rigorous enforcement of thermal equipartition. For example, stiff improper dihedral and/or angle potentials are utilized to constrain the planarity of sp<sup>2</sup> carbon in the acetone and imidazolium cation studied here. The effective temperature of these "constrained" DOF is not important for most liquid-state properties of interest, although the resulting high-frequency modes may overlap with the Drude oscillator power spectrum and promote heat flow. To properly simulate such systems, we introduce a new thermostat algorithm that separates out the molecular translational (center of mass, CM) DOF from the intramolecular DOF as well as from the electronic DOF. This is similar to the pioneering work of Sprik on bulk water, 18 and we suggest that such a scheme is generally advantageous for polarizable simulations of non-rigid molecules. As we demonstrate below, this temperature grouped dual-Nosé-Hoover (tgNH) thermostat properly describes both static and dynamic properties for all the systems tested here as benchmarked against a SCF polarization treatment; importantly, the results are rather insensitive to the coupling strength.

In Figure 1, diffusion coefficients are presented for the four systems predicted with the dual-LV, dual-NH, and tgNH schemes as functions of thermostat coupling constant, and the results illustrate that the fidelity of different dual-temperature thermostat schemes can be very system dependent. With the LV (dual) thermostat, for all systems studied here, translational diffusion is significantly reduced compared to simulations with the SCF scheme, especially with decreasing coupling time. While this effect is similar to that observed in non-polarizable simulations,  $^{23}$  it is more severe for the polarizable acetone and  $\rm BMIM^+BF_4^-$  simulations.

With the dual-NH thermostat, for water and NaCl/water systems, which contain no intramolecular degrees of freedom (rigid water model), the results are excellent. For acetone and  $\mathrm{BMIM}^+\mathrm{BF}_4^-$ , however, the dual-NH thermostat exhibits equipartition problems with too high translational kinetic energies (vide infra), resulting in overestimated diffusion coefficients as shown in Figure 1c-d. The dual-NH scheme is thus only appropriate in the absence of high-frequency, intramolecular modes. Note that this behavior is absent in non-polarizable simulations, since it results from heat flow introduced by coupling between the high-frequency modes and the Drude oscillator DOF.

We also note that while the predicted diffusion is not affected much by the coupling time  $\tau$  with the dual-NH scheme, applying different constraints on the bonds have a significant impact on the computed D. In Figures 1, 2 and 4, bonds containing hydrogen (C-H bonds in acetone and BMIM<sup>+</sup>BF<sub>4</sub><sup>-</sup>) are constrained, while other bonds are not. As shown in the supporting information (SI Figure S6), con-

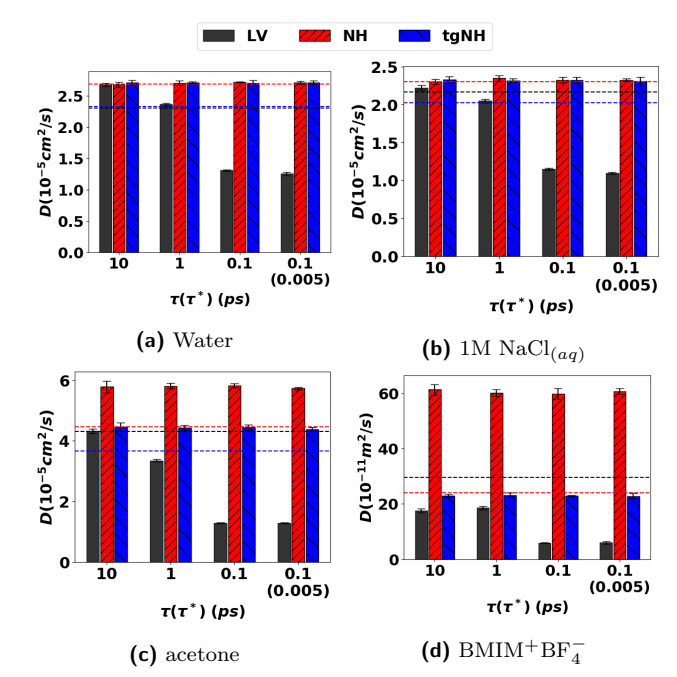


Figure 1. Self-diffusion coefficient (D) of (a) pure water, (b) water in 1M NaCl $_{(aq)}$  (c) acetone and (d) BMIM $^+$ BF $_4^-$  calculated with different thermostats; finite size correction of Yeh and Hummer  $^{27}$  is included for all computed D values.  $\tau$  and  $\tau^*$  are the coupling time to the heat bath for the real and Drude DOF, respectively. For (c) and (d), simulations are performed at the experimental density of acetone  $(784~kg/m^3)^{28}$  and BMIM $^+$ BF $_4^-$ (1130  $kg/m^3$ ), $^{29}$  respectively. Black: dual-LV, red: dual-NH, blue: tgNH thermostat. Black horizontal lines: experimental values, $^{28-31}$  blue and red horizontal lines indicate literature values calculated with the SCF scheme  $^{31-34}$  without and with finite size correction, $^{27}$  respectively. SCF scheme results were obtained with NVE simulations except for BMIM $^+$ BF $_4^-$ , which was calculated with the single Nosé-Hoover thermostat implemented in the GROMACS simulation package. $^{35}$  The error bars are shown in black and are typically less than 2%.

straining all bonds to their equilibrium lengths improves the predicted D over constraining only C-H bonds. Allowing C-H bonds to be flexible greatly worsens the overestimation in D. As discussed below, the dual-NH thermostat also significantly underestimates the densities of non-aqueous systems, which further aggravates the problem of overestimated diffusion. These limitations of the dual-NH thermostat have been largely overlooked in the literature since the initial development focused on constrained water models that did not have any high-frequency internal DOF.

With the tgNH thermostat, diffusion coefficients show remarkable agreement with literature values obtained with the SCF scheme for all four systems. Moreover, the predicted D is essentially invariant to the coupling strength to the heat bath, indicating the robustness of temperature control. The excellent performance of the tgNH thermostat is due to the separate coupling of translational and intramolecular DOF, so that equipartition problems for high frequency modes do not affect molecular translational motions.

We note that the calculated self diffusion coefficients of water and acetone experience significant finite-size effects, thus the correction suggested by Yeh and Hummer  $^{27}$  must be included when comparing with experiments or simulations with different system sizes. While the reported self-diffusion coefficient of SWM4-NDP  $^{32}$  ( $D=2.33\times 10^{-5}cm^2/s$ ) agrees well with experiment, it was calculated

with a very small system size (250 water molecules) and the model actually overestimates water diffusion when finite size effects are properly accounted for (red dotted line in Fig. 1a). <sup>36</sup> Interestingly, the reported diffusion of SAPT-FF for acetone was slower than the experiment, <sup>33</sup> but the finite size correction significantly improves the agreement (Fig. 1c), despite omitting the three body interaction which was shown to be important for density prediction. <sup>33</sup> The finite size correction for BMIM $^+$ BF $^-_4$  is negligible due to the high viscosity of the system (Fig. 1d).

For the prediction of system density, we note that results of the dual-LV thermostat strongly depend on the coupling strength  $\tau$ , while those of dual-NH and tgNH thermostats do not show much  $\tau$  dependence (SI Figures S1-S4). In Figure 2, the influence of thermostats on the density ( $\rho$ ) and apparent temperature of the real particles ( $T_R$ , Eq. 14), Drude particles ( $T_D$ , Eq. 15), and molecular center of mass ( $T_{CM}$ , Eq. 13) DOF is shown by using the weakly coupled case ( $\tau = \tau^* = 10ps$ ) as an example. For aqueous systems, density results are largely insensitive to the thermostat and in good agreement with experiment, consistent with trends for the diffusion coefficients shown in Figure 1. Similarly, temperature equipartition is satisfied for  $T_{CM}$ , while  $T_D$  is maintained at a low temperature, with most thermostat choices.

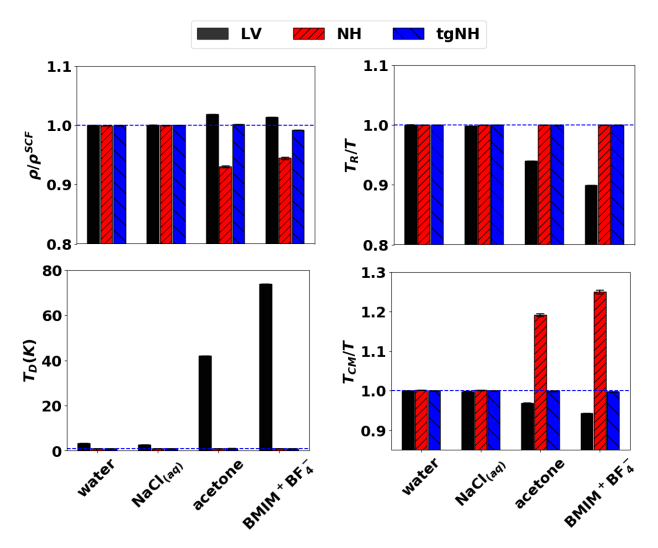


Figure 2. Static properties predicted with different thermostats using a weak coupling  $(\tau = \tau^* = 10ps)$  to the heat bath.  $\rho/\rho^{SCF}$ : system density  $(\rho)$  normalized by the predictions of the SCF scheme  $(\rho^{SCF})$ ;  $T_R$ : apparent system temperature (all real particles DOF);  $T_D$ : effective temperature of the Drude DOF;  $T_{CM}$ : effective temperature of CM translational motions; thermostat temperature T is set at 298 K for all systems except for BMIM $^+$ BF $_4^-$ , which is set at 400 K; blue dotted line represents the reference value of 1.0.

For acetone and BMIM<sup>+</sup>BF<sub>4</sub><sup>-</sup> systems, by contrast, substantial variations in predicted density and temperature decomposition are observed with different thermostats. Most notably, the dual-NH thermostat significantly underestimates the densities of acetone and BMIM<sup>+</sup>BF<sub>4</sub><sup>-</sup> with all tested coupling strengths (see also SI Figures S3-S4) compared to benchmark values obtained with the SCF scheme. <sup>33,34</sup> This is because the molecular center of mass temperatures ( $T_{CM}$ ) are much too high, which compensate for the low temperatures within the high frequency, intramolecular modes (see below). On the other hand, the weakly coupled dual-LV thermostat with  $\tau = 10ps$  overestimates the system density for acetone and BMIM<sup>+</sup>BF<sub>4</sub><sup>-</sup>, due

to underestimated system temperature  $(T_R)$ , in particular,  $T_{CM}$ . Inspection of  $T_D$  clearly indicates the reason for this behavior, as there is substantial heat flow to the Drude DOF when using such a weak coupling constant. Coupling constants of  $\tau < 1ps$  for the dual-LV thermostat are thus necessary for simulations of acetone, BMIM<sup>+</sup>BF<sub>4</sub><sup>-</sup> and similar systems with high-frequency, intramolecular modes. Among the three thermostat schemes, only the tgNH thermostat shows excellent agreement with the SCF scheme for all systems regardless of the coupling strength to the heat bath.

The significant error of the dual-NH thermostat in density for acetone and BMIM<sup>+</sup>BF<sub>4</sub> is due to an incorrect partitioning of the kinetic energy: the CM translational effective temperatures  $(T_{CM})$  are much higher than the set temperature (350 K vs. 298 K for acetone and 500 K vs. 400 K for BMIM<sup>+</sup>BF<sub>4</sub>); note that only the apparent system temperature for both real particles  $(T_R)$  and Drude  $(T_D)$  DOF are rigorously maintained at the set temperatures. As shown in Figure 3, the molecular center of mass temperature  $(T_{CM})$ largely dictates the density and liquid state properties, and the system effectively behaves as if it were at a higher temperature, while  $T_R$  is essentially artificial when equipartition is violated. The dual-LV thermostat does not exhibit the same problem because of the rigorous partitioning of kinetic energy to all atoms. This holds even for the weakly coupled case with  $\tau = 10ps$ ;  $T_R$  and  $T_{CM}$  are similar although both are lower than the set temperature, leading to higher predicted densities. The tgNH thermostat avoids the problem by putting a separate thermostat on the CM translational DOF, stabilizing both  $T_R$  and  $T_{CM}$  at the set temperature T and  $T_D$  at  $T^*$ , respectively.

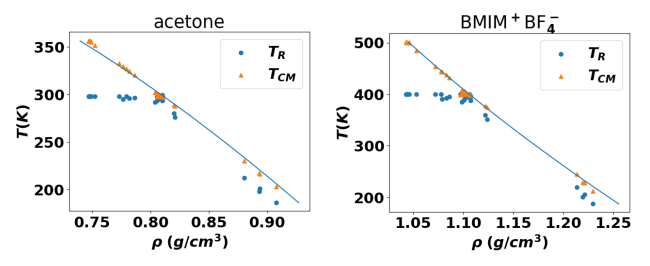


Figure 3. Correlation between the predicted system density and the apparent system temperature  $(T_R)$  and effective temperature of CM translational motion  $(T_{CM})$  for acetone and BMIM<sup>+</sup>BF $_4$ The data are based on combined results of simulations with different thermostats, including the type of thermostat scheme, coupling strength, bond constraints, as well as use of chain variables (see SI). The lines are fits to the thermal expansion equation.

Another fundamental distinction among the thermostats tested here is that the velocity-randomizing dual-LV thermost fails to keep the Drude temperature at 1 K, while velocity-rescaling dual-NH and tgNH thermostats equilibrate the system at the desired temperature for both (apparent) real and Drude DOF. While the effect is minimal in aqueous systems ( $T_D \leq 3K$ , Figure 2),  $T_D$  can reach as high as 70 K for BMIM<sup>+</sup>BF<sub>4</sub> with a weak coupling to the heat bath in the dual-LV thermostat. In SI Figures S1-S4 we show predictions from a dual-LV thermostat with unequal choices of real DOF ( $\tau = 0.1ps$ ) and Drude DOF  $(\tau^* = 0.005ps)$  coupling constants. This comparison is included because prior literature sometimes reports the use of a stronger coupling for the Drude DOF than the real DOF, to ensure the Drude DOF to stay near the minimum energy state. Although this dual-LV setting has the intended effect of maintaining the Drude temperature closer to the set

value of 1 K, it has the undesired consequence of lowering the temperatures of the real DOF ( $T_R$  and  $T_{CM}$ ). We thus suggest that dual-LV thermostat be utilized only with equal coupling strength to both heat baths.

The artificially high Drude temperatures that may arise with dual-LV thermostat are due to the internal heat flow from higher temperature DOF of the real atoms, specifically the high-frequency modes. This is in contrast to simulations employing only one thermostat, in which case the (single) LV thermostat is often considered the stronger coupling scheme, mediating more efficient equilibration and robust equipartition compared to a (single) NH thermostat. The difference in the dual-LV thermostat scheme is that each of the atom-Drude pairs is coupled to two heat baths, and there is intrinsic heat flow from the real to the Drude DOF. This heat transfer is not balanced with the stochastic recovering force, and results in a higher  $T_D$  than the set temperature  $T^*$  (1 K) and a lower  $T_R$  than the set temperature T. The heat flow is strongly dependent on the frequency of the motion; high frequency internal DOF, such as C-H stretch vibrations or the improper dihedrals of acetone and BMIM<sup>+</sup>BF<sub>4</sub>, lose considerable kinetic energy to the Drude DOF. To keep the Drude  $T_D$  at the set temperature  $T^*$  for these systems, the fluctuation-dissipation relation in Eq. 5 (see Methods) needs to be modified to account for the amount of the internal heat transfer, which is system dependent. A strong coupling  $(\tau = 0.1ps)$  is desirable to keep the system at the set temperatures T and  $T^*$ , but this significantly alters dynamics as discussed above.

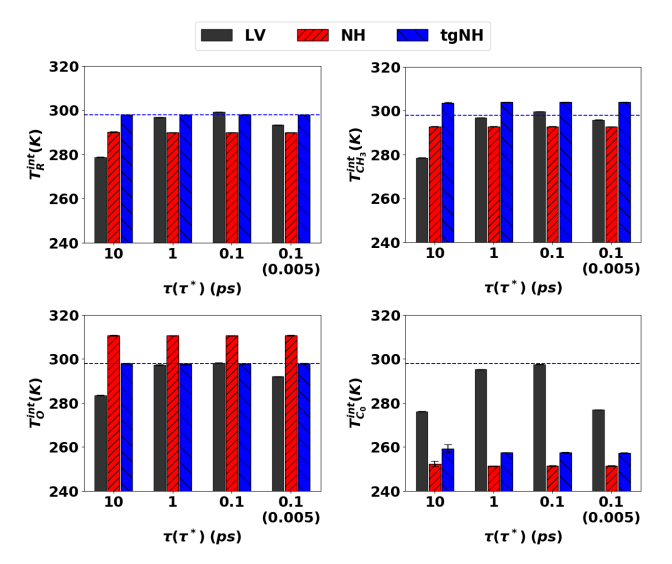


Figure 4. The effect of the thermostats on the effective temperature representing intramolecular (int) motions associated with different atoms in acetone.  $T_R^{int}$ : temperature of total intramolecular real particles DOF;  $T_{CH_3}^{int}$ : temperature of  $CH_3$  groups;  $T_O^{int}$ : temperature of the oxygen atoms;  $T_{C_0}^{int}$ : temperature of the central carbon atoms. The blue dotted line shows the set temperature of 298 K.

With velocity rescaling dual-NH and tgNH thermostats, the heat flow from the real to Drude DOF does not affect the apparent real and Drude temperatures  $T_R$  and  $T_D$ . These thermostats explicitly couple the real and Drude DOF to the respective heat bath at T and  $T^*$ , respectively. The potential problem is that equipartitioning of kinetic energy is not guaranteed, since each thermostat mass Q and  $Q^*$  involves a large number of DOF. The internal heat flow generates a stationary temperature gradient among different motions.

For the dual-NH thermostat, the loss of kinetic energy in the high frequency modes to the Drude modes leads to a higher kinetic energy in the low frequency motions to balance the fixed net temperature,  $T_R$  (e.g., a high  $T_{CM}$ , Figure 2). This results in significantly underestimated densities and overestimated diffusion coefficients, as  $T_{CM}$  reaches 50 K and 100 K above the set temperature T for acetone and BMIM<sup>+</sup>BF<sub>4</sub>, respectively.

In Figure 4, we further analyze these equipartition problems by examining the temperature of various intramolecular modes for the acetone simulations performed at the experimental density. Specifically, we show the temperatures of intramolecular motions for the carbonyl oxygen  $(T_O^{int})$ , carbonyl carbon  $(T_{C_0}^{int})$ , methyl groups  $(T_{CH_3}^{int})$ , and total intramolecular DOF  $(T_R^{int})$  of acetone, with the different thermostat schemes. With the dual-NH schemes, the carbonyl carbon " $C_0$ " is responsible for the most kinetic energy loss to the Drude DOF. This is due to the strong coupling between the Drude oscillator modes and the high-frequency modes generated by the improper dihedral and angle potentials centered at  $C_0$ . The effective temperature  $T_{C_0}^{int}$  is 50 K below the set temperature, which balances the 50 K higher  $T_{CM}$  over T. Similarly, the nitrogen and carbon atoms in the ring of BMIM<sup>+</sup>BF<sub>4</sub> lose the most kinetic energy to the Drude DOF (SI Figure S7). When the C-H bonds are not constrained, the high frequency C-H vibrations also lose significant kinetic energy to the Drude DOF (SI Figure S5).

The essential difference between the dual-NH and tgNH schemes is reflected by the  $T_R^{int}$  profile in Figure 4. Because the tgNH thermostat employs separate heat baths for translational and intramolecular motions,  $T_R^{int}$  is maintained at the desired temperature for all coupling constants  $\tau$ , despite the low  $T_{C_0}^{int}$ . The low  $T_{C_0}^{int}$  is compensated by the slightly higher  $T_{CH_3}^{int}$ , while  $T_{CM}$  remains unaffected. Note the different numbers of DOF within  $T_{CH_3}^{int}$  and  $T_{C_0}^{int}$  groups, which is the reason that temperature deviations are not of the same magnitude. Such temperature compensation within the intramolecular DOF, being separate from the translational DOF, is preferable to the dual-NH scheme, as evident in the density and diffusion coefficient benchmarks (Figures 1 and 2). If better equipartition of intramolecular motions is desired, one could further set individual thermostats for different atom types using Eq. 16. This would be useful for calculating spectroscopic properties which are strongly dependent on the vibrational motion of each bond.

In summary, we show that conventional dual-temperature thermostat schemes for polarizable simulations often fail to enforce rigorous equipartition and adiabatic electronic state if high frequency, intramolecular modes are present. The most severe errors in static and dynamic properties are observed when the dual-NH thermostat is utilized for simulations of acetone and BMIM<sup>+</sup>BF<sub>4</sub>; substantially higher effective temperatures for translational motions lead to significantly underestimated densities and overestimated diffusion coefficients. While only dual-LV thermostat with strong coupling  $(\tau < 1ps)$  rigorously ensures equipartition for the high frequency, intramolecular motions, this scheme leads to significantly damped dynamic properties. Dual-LV thermostat with a weak coupling  $(\tau > 1ps)$  is also problematic as the cold temperature of the Drude DOF is not maintained. Our proposed tgNH thermostat resolves these problems by explicitly coupling separate heat baths to the translational and intramolecular motions, while maintaining a significant speed-up over the iterative SCF scheme. Any equipartition problems caused by heat flow to the Drude DOF are internally compensated by temperatures of the other intramolecular modes, and the strict enforcement of translational temperature enables robust prediction of both static and dynamic properties with minimal dependence on the magnitude of the coupling parameter. We anticipate that our method will find a broad range of applicability to systems of biological and industrial relevance where electronic polarization plays important roles.

Methods: All simulations are performed with an extensible molecular dynamics toolkit OpenMM version 7.2, 15 of which the performance is optimized with massive parallelization utilizing graphical processing units (GPUs). A custom OpenMM plugin to perform dual-NH and tgNH integrations is developed in this work and is readily available for downloaded from https://github.com/scychon/ openmm\_drudeNose. The CHARMM Drude polarizable force field 37 based on the SWM4-NDP water model 32 is utilized for water and NaCl. 38 For acetone and BMIM<sup>+</sup>BF<sub>4</sub>, we use the recently developed first-principles force fields parametrized based on symmetry adapted perturbation theory (SAPT-FF)<sup>33,34</sup> for nonbonded interactions; bond, angle and dihedral parameters are taken from OPLS all atom force fields. <sup>39,40</sup> The SAPT-FF was shown to predict both the static and dynamic properties of these systems accurately without any empirical adjustment and has also been successfully applied to highly charged and interfacial systems. <sup>7,41</sup> Details of composition and simulation parameters for the systems studied here are summarized in Supporting Information (SI).

In dual-temperature thermostat schemes for the Drude oscillator model, each Drude particle is assigned with a small mass  $(m_D; 0.4 \text{ amu} \text{ used in this study})$  that is subtracted from its parent particle, thus the mass of atom-Drude pair sums to the original mass of the atom  $(m_i)$ . During the integration, the first thermostat for the real system temperature (T) regulates the motion of the center of mass of atom-Drude pairs  $(\mathbf{R}_i)$ , and the second thermostat with a low temperature  $(T^* \ll T)$  regulates the relative motion of Drude particles to their parent atoms  $(\mathbf{d}_i)$ . For non-polarizable atoms without Drude particles (usually hydrogen),  $\mathbf{R}_i$  indicates the atomic position and  $\mathbf{d}_i$  is ignored. Forces on  $\mathbf{R}_i$  and  $\mathbf{d}_i$  are calculated using the absolute positions of the parent  $(\mathbf{r}_i)$  and Drude particles  $(\mathbf{r}_{D,i})$  as,

$$\mathbf{F}_{\mathbf{R},i} = -\frac{\partial U}{\partial \mathbf{r}_{i}} - \frac{\partial U}{\partial \mathbf{r}_{D,i}},\tag{1}$$

$$\mathbf{F}_{\mathbf{d},i} = \left(\frac{m_D}{m_i}\right) \frac{\partial U}{\partial \mathbf{r}_i} - \left(1 - \frac{m_D}{m_i}\right) \frac{\partial U}{\partial \mathbf{r}_{D,i}}.$$
 (2)

The equations of motion for the dual-LV thermostat are,

$$m_i \ddot{\mathbf{R}}_i = \mathbf{F}_{\mathbf{R},i} - m_i \gamma \dot{\mathbf{R}}_i + \mathbf{f}_i, \tag{3}$$

$$m_i' \ddot{\mathbf{d}}_i = \mathbf{F}_{\mathbf{d},i} - m_i' \gamma' \dot{\mathbf{d}}_i + \mathbf{f}_i', \tag{4}$$

where  $m_i' = m_D(1 - m_D/m_i)$  is the reduced mass of the atom-Drude pair. The coupling to heat baths is modeled with the Langevin friction coefficients  $\gamma$  and  $\gamma'$ , which are related with the coupling relaxation times  $\tau = 1/\gamma$  and  $\tau^* = 1/\gamma'$ . The fluctuating random forces  $\mathbf{f}_i$  and  $\mathbf{f}_i'$  obey the fluctuation-dissipation theorem,

$$\mathbf{f}_{i} = (2\gamma k_{B}T/m_{i})^{1/2}R(t),$$
  

$$\mathbf{f}'_{i} = (2\gamma' k_{B}T^{*}/m'_{i})^{1/2}R^{*}(t),$$
(5)

where R(t) and  $R^*(t)$  are univariate Gaussian random pro-

cesses and  $k_B$  is the Boltzmann constant.

In the dual-NH thermostat, the equations of motion are,

$$m_i \ddot{\mathbf{R}}_i = \mathbf{F}_{\mathbf{R},i} - m_i \dot{\mathbf{R}}_i \dot{\eta},\tag{6}$$

$$m_i' \ddot{\mathbf{d}}_i = \mathbf{F}_{\mathbf{d},i} - m_i' \dot{\mathbf{d}}_i \dot{\eta}^*, \tag{7}$$

$$Q\ddot{\eta} = \sum_{j}^{N} m_j \dot{R}_j^2 - N_f k_B T, \tag{8}$$

$$Q^* \ddot{\eta}^* = \sum_{j}^{N} m'_j \dot{d}_j^2 - N_f^* k_B T^*.$$
 (9)

The summation runs over N particles including both the atom-Drude pairs and the non-polarizable atoms.  $N_f$  is the number of DOF associated with the atomic motion and should account for the number of distant constraints  $(n_c)$  such that  $N_f = 3N - n_c$ .  $N_f^* = 3N_D$  is the number of DOF associated with the internal motion of  $N_D$  atom-Drude pairs. Q and  $Q^*$  are thermal inertia parameters for NH thermostat and are related to the characteristic time scales of the motion,  $\tau$  and  $\tau^*$ , via  $Q = N_f k_B T \tau^2$  and  $Q^* = N_f^* k_B T^* \tau^{*2}$ . The thermal velocities  $\dot{\eta}$  and  $\dot{\eta}^*$  act as scaling exponents on the velocities  $\dot{R}_i$  and  $\dot{d}_i$ . Multiple timestep algorithm proposed by Martyna et al.  $^{42}$  is also used such that multiple NH moves (we use 20 per atomic move) of inertia are made per integration of atomic move.

The tgNH thermostat developed in this work assigns an independent thermostat to the center of mass (CM) translational motions of each molecule. The equation of motion for the thermal inertia of the real DOF (Eq. 8) is further divided into CM DOF and internal (int) DOF,

$$Q_{CM}\ddot{\eta}_{CM} = \sum_{i}^{N_{mol}} M_i \dot{R}_{CM,i}^2 - 3N_{mol}k_B T,$$
 (10)

$$Q_{int}\ddot{\eta}_{int} = \sum_{j}^{N} m_{j} \dot{R}_{int,j}^{2} - (N_{f} - 3N_{mol})k_{B}T,$$

$$\dot{R}_{int,j} = \dot{R}_{j} - \dot{R}_{CM,i}.$$
(11)

where the first summation runs over the total number of molecules  $(N_{mol})$ , and the second summation runs over N particles as in Eq. 8.  $3N_{mol}$  represents the total translational DOF for  $N_{mol}$  molecules, and  $N_f - 3N_{mol}$  represents the remaining internal DOF of real particles. The thermal velocity scaling factors,  $\dot{\eta}_{CM}$  and  $\dot{\eta}_{int}$ , are determined by the corresponding thermal inertia parameters,  $Q_{CM} = 3N_{mol}k_BT\tau^2$  and  $Q_{int} = (N_f - 3N_{mol})k_BT\tau^2$ . Now the equation of motion for real particle j in a molecule i corresponding to Eq. 6 becomes,

$$m_j \mathbf{\ddot{R}}_j = \mathbf{F}_{\mathbf{R},j} - m_j \left( \mathbf{\dot{R}}_{\mathbf{CM},i} \dot{\eta}_{CM} + \mathbf{\dot{R}}_{int,j} \dot{\eta}_{int} \right). \tag{12}$$

In addition to the molecular translational DOF, one can separate out any arbitrary DOF to a separate temperature group. Eqs. 10-12 are easily extended to such a case, by adding more thermal velocity terms and corresponding thermal inertia parameters for each additional temperature group.

To characterize the equipartitioning of kinetic energy into different DOF, we define four types of effective temperatures: CM translational temperature  $(T_{CM})$ , total real particle temperature  $(T_R)$ , total Drude temperature  $(T_D)$ , and particle internal temperature  $(T_{R(\alpha)}^{int})$  for each atom type  $\alpha$ . These effective temperatures are defined in terms of their

associated DOF,

$$T_{CM} = \frac{\sum_{i}^{N_{mol}} M \dot{R}_{CM,i}^2}{3N_{mol}k_B},$$
 (13)

$$T_R = \frac{\sum_i^N m_i \dot{R}_i^2}{N_f k_B},\tag{14}$$

$$T_D = \frac{\sum_{i}^{N_D} m_i' \dot{d}_i^2}{3N_D k_B},\tag{15}$$

$$T_{R(\alpha)}^{int} = \frac{\sum_{i}^{N(\alpha)} m_i \left( \dot{R}(\alpha)_i - \dot{R}_{CM;i} \right)^2}{(3 \sum_{i}^{N(\alpha)} (1 - m_i/M) - n_c(\alpha)) k_B}.$$
 (16)

Here M is the mass of the molecule and  $m_i$  is the mass of ith atom-Drude pair or a non-polarizable atom,  $N(\alpha)$  represents the number of atom-Drude pairs and/or the non-polarizable atoms corresponding to an atom group  $\alpha$ ,  $R(\alpha)_i$  represents the position of the center of mass of ith atom-Drude pair or the position of ith non-polarizable atom,  $R_{CM;i}$  represents the center of mass of the molecule containing ith atom,  $N_D$ represents the number of atom-Drude pairs, and  $m'_i$  and  $d_i$ represents the reduced mass and the relative distance vector of ith atom-Drude pair. When a molecule is modeled with constraints such as O-H bonds in the rigid water model, the atoms in a constraint should be placed to the same atom group, and  $n_c(\alpha)$  represents the number of such constraints belonging to the atom group  $\alpha$ . An ideal thermostat that satisfies the equipartitioning theorem should equilibrate the system at the desired temperature such that  $T_R = T_{CM} =$  $T_{R(\alpha)}^{int} = T$  and  $T_{D(\alpha)} = T^*$  for all groups  $\alpha$ .

This work was supported in part by US Department of Energy, Basic Energy Sciences under grant DE-SC0017877, the University of Wisconsin Materials Research Science and Engineering Center under grant DMR-1121288, the National Science Foundation under grant CHE-1664906 and grant CHE-1829555. Computational resources were provided by the Center for High Throughput Computing at the University of Wisconsin and the Extreme Science and Engineering Discovery Environment (XSEDE), 43 which is supported by National Science Foundation grant number ACI-1548562. We also acknowledge NVIDIA Corporation for the donation of Titan Xp GPU card used for this research.

Supporting Information Available: Details of simulation protocols including system preparation, thermostat parameters and calculation of thermodynamic quantities; discussions about the effect of using NH-Chain, bond constraints, dual canonical sampling through velocity rescaling (dual-CSVR) thermostat; predictions of rotational relaxation time and dielectric constants for acetone; benchmark of simulation performance of each thermostat scheme.

## References

- (1) Lemkul, J. A.; Huang, J.; Roux, B.; MacKerell, A. D. An Empirical Polarizable Force Field Based on the Classical Drude Oscillator Model: Development History and Recent Applications. Chem. Rev. 2016, 116, 4983-5013.
- McDaniel, J. G.; Yethiraj, A. Influence of Electronic Polarization on the Structure of Ionic Liquids. J. Phys. Chem. Lett.
- 2018, 9, 4765–4770. Son, C. Y.; McDaniel, J. G.; Schmidt, J. R.; Cui, Q.; Yethiraj, A. First-Principles United Atom Force Field for the Ionic Liquid BMIM<sup>+</sup>BF<sub>4</sub>: An Alternative to Charge Scaling. *J. Phys. Chem. B* **2016**, *120*, 3560–3568.
  Choi, E.; Yethiraj, A. Entropic Mechanism for the Lower Crit-
- ical Solution Temperature of Poly(ethylene oxide) in a Room Temperature Ionic Liquid. ACS Macro Lett. 2015, 4, 799–803.
- Salanne, M. Simulations of Room Temperature Ionic Liquids: From Polarizable to Coarse-Grained Force Fields. Phys. Chem.
- Chem. Phys. 2015, 17, 14270–14279. Okur, H. I.; Hladílková, J.; Rembert, K. B.; Cho, Y.; Heyda, J.; Dzubiella, J.; Cremer, P. S.; Jungwirth, P. Beyond the Hofmeis-

- ter Series: Ion-Specific Effects on Proteins and Their Biological Functions. J. Phys. Chem. B 2017, 121, 1997–2014.
- McDaniel, J.; Son, C. Ion Correlation and Collective Dynamics in BMIM/BF<sub>4</sub>-Based Organic Electrolytes: From Dilute Solutions to the Ionic Liquid Limit. J. Phys. Chem. B 2018, 122, 7154-7169.
- Huang, J.; MacKerell, A. D. Induction of Peptide Bond Dipoles Drives Cooperative Helix Formation in the (AAQAA)<sub>3</sub> Peptide. Biophys. J. **2014**, 107, 991–997.
- Halgren, T. A.; Damm, W. Polarizable Force Fields. Curr. Opin. Struct. Biol. 2001, 11, 236–242.

  Warshel, A.; Kato, M.; Pisliakov, A. V. Polarizable Force Fields: History, Test Cases, and Prospects. J. Chem. Theory Comput. 2007, 3, 2034–2045.
- (11) Huang, J.; Lopes, P. E. M.; Roux, B.; MacKerell, A. D. Recent Advances in Polarizable Force Fields for Macromolecules: Microsecond Simulations of Proteins Using the Classical Drude
- Oscillator Model. J. Phys. Chem. Lett. 2014, 5, 3144–3150. Baker, C. M. Polarizable Force Fields for Molecular Dynamics Simulations of Biomolecules. Wiley Interdiscip. Rev. Comput. **2015**, 5, 241-254.
- Lamoureux, G.; Roux, B. Modeling Induced Polarization with Classical Drude Oscillators: Theory and Molecular Dynamics Simulation Algorithm. J. Chem. Phys. 2003, 119, 3025–3039. (14) Jiang, W.; Hardy, D. J.; Phillips, J. C.; MacKerell, A. D.; Schul-
- ten, K.; Roux, B. High-Performance Scalable Molecular Dynamics Simulations of a Polarizable Force Field Based on Classical Drude Oscillators in NAMD. J. Phys. Chem. Lett. 2011, 2, 87 - 92.
- (15) Eastman, P.; Swails, J.; Chodera, J. D.; McGibbon, R. T.; Zhao, Y.; Beauchamp, K. A.; Wang, L. P.; Simmonett, A. C.; Harrigan, M. P.; Stern, C. D.; et al., OpenMM 7: Rapid Development of High Performance Algorithms for Molecular Dynamics. *PLoS Comput. Biol.* **2017**, *13*, e1005659.
- (16) Sherwood, P.; de Vries, A. H.; Guest, M. F.; Schreckenbach, G.; Catlow, C. R. A.; French, S. A.; Sokol, A. A.; Bromley, S. T.; Thiel, W.; Turner, A. J.; et al., QUASI: A General Purpose Implementation of the QM/MM Approach and Its Application to Problems in Catalysis. J. Mol. Struct.: THEOCHEM 2003, 632, 1-28.
- (17) Lemkul, J. A.; Roux, B.; van der Spoel, D.; MacKerell, A. D. Implementation of Extended Lagrangian Dynamics in GROMACS for Polarizable Simulations Using the Classical Drude Oscillator Model. J. Comput. Chem. 2015, 36, 1473–1479.
- Sprik, M. Computer Simulation of the Dynamics of Induced Polarization Fluctuations in Water. J. Phys. Chem. 1991, 95, 2283-2291
- Fois, E. S.; Penman, J. I.; Madden, P. A. Control of the Adiabatic Electronic State in Ab Initio Molecular Dynamics . J. Chem. Phys. 1993, 98, 6361.
- Lingenheil, M.; Denschlag, R.; Reichold, R.; Tavan, P. The "Hot-Solvent/Cold-Solute" Problem Revisited. J. Chem. The-
- Froblem Revisited. J. Chem. Theory Comput. 2008, 4, 1293–1306.
  Eastwood, M. P.; Stafford, K. A.; Lippert, R. A.; Jensen, M.; Maragakis, P.; Predescu, C.; Dror, R. O.; Shaw, D. E. Equipartition and the Calculation of Temperature in Biomolecular Simulations. J. Chem. Theory Comput. 2010, 6, 2045–2058.
- (22) Leimkuhler, B.; Noorizadeh, E.; Penrose, O. Comparing the Efficiencies of Stochastic Isothermal Molecular Dynamics Methods.
- J. Stat. Phys. 2011, 143, 921–942.
  Basconi, J. E.; Shirts, M. R. Effects of Temperature Control Algorithms on Transport Properties and Kinetics in Molecular Dynamics Simulations. J. Chem. Theory Comput. 2013, 9, 2887-2899.
- Palmer, J. C.; Car, R.; Debenedetti, P. G. The Liquid-Liquid Transition in Supercooled ST2 Water: A Comparison Between Umbrella Sampling and Well-Tempered Metadynamics. Faraday Discuss. 2013, 167, 77–94.
- (25) Limmer, D. T.; Chandler, D. The Putative Liquid-Liquid Transition Is a Liquid-Solid Transition in Atomistic Models of Water.
- II. J. Chem. Phys. 2013, 138.

  Palmer, J. C.; Haji-Akbari, A.; Singh, R. S.; Martelli, F.; Car, R.; Panagiotopoulos, A. Z.; Debenedetti, P. G. Comment on "The Putative Liquid-Liquid Transition Is a Liquid-Solid Transition in Atomistic Models of Water" [I and II: J. Chem. Phys. 135, 134503 (2011); J. Chem. Phys. 138, 214504 (2013)].
- J. Chem. Phys. 2018, 148, 137101. Yeh, I. C.; Hummer, G. System-Size Dependence of Diffusion Coefficients and Viscosities From Molecular Dynamics Simulations with Periodic Boundary Conditions. J. Phys. Chem. B **2004**, 108, 15873-15879.
- Ahn, C. B.; Lee, S. Y.; Nalcioglu, O.; Cho, Z. H. An Improved Nuclear Magnetic Resonance Diffusion Coefficient Imaging Method Using an Optimized Pulse Sequence. Med. Phys. **1986**, *13*, 789–793.
- Tokuda, H.; Hayamizu, K.; Ishii, K.; Bin, A.; Susan, H.; Watanabe, M. Physicochemical Properties and Structures of Room Temperature Ionic Liquids. 1. Variation of Anionic Species. J. Phys. Chem. B 2004, 108, 16593–16600. Krynicki, K.; Green, C. D.; Sawyer, D. W. Pressure and Temper-
- ature Dependence of Self-Diffusion in Water. Faraday Discuss. Chem. Soc. 1978, 66, 199–208.
- Kim, J. S.; Wu, Z.; Morrow, A. R.; Yethiraj, A.; Yethiraj, A. Self-Diffusion and Viscosity in Electrolyte Solutions. *J. Phys.*

- Chem. B **2012**, 116, 12007–12013. Lamoureux, G.; Harder, E.; Vorobyov, I. V.; Roux, B.; MacKerell, A. D. A Polarizable Model of Water for Molecular Dynamics Simulations of Biomolecules. Chem. Phys. Lett. 2006, 418, 245-249
- (33) McDaniel, J. G.; Schmidt, J. R. First-Principles Many-Body Force Fields From the Gas Phase to Liquid: A "Universal" Ap-proach. J. Phys. Chem. B 2014, 118, 8042–8053.
- Choi, E.; McDaniel, J. G.; Schmidt, J. R.; Yethiraj, A. First-Principles, Physically Motivated Force Field for the Ionic Liquid
- [BMIM][BF<sub>4</sub>]. J. Phys. Chem. Lett. **2014**, 5, 2670–2674. Pronk, S.; Páll, S.; Schulz, R.; Larsson, P.; Bjelkmar, P.; Apostolov, R.; Shirts, M. R.; Smith, J. C.; Kasson, P. M.; van der Spoel, D.; Hess, B.; Lindahl, E. GROMACS 4.5: A High-Throughput and Highly Parallel Open Source Molecular Simulation Toolkit. Bioinformatics 2013, 29, 845–854.
- Yu, W.; Lopes, P. E. M.; Roux, B.; MacKerell, A. D. Six-site Polarizable Model of Water Based on the Classical Drude Oscillator. *J. Chem. Phys.* **2013**, *138*, 034508.

  Lopes, P. E. M.; Huang, J.; Shim, J.; Luo, Y.; Li, H.; Roux, B.;
- MacKerell, A. D. Polarizable Force Field for Peptides and Proteins Based on the Classical Drude Oscillator. J. Chem. Theory Comput. **2013**, 9, 5430–5449.
- Yu, H.; Whitfield, T. W.; Harder, E.; Lamoureux, G.; Vorobyov, I.; Anisimov, V. M.; MacKerell, A. D.; Roux, B. Simulating Monovalent and Divalent Ions in Aqueous Solution Using a Drude Polarizable Force Field. J. Chem. Theory Comput.
- 2010, 6, 774–786. (39) Jorgensen, W. L.; Maxwell, D. S.; Tirado-Rives, J. Development and testing of the OPLS all-atom force field on conformational energetics and properties of organic liquids. J. Am. Chem. Soc. **1996**, 118, 11225–11236.
- Sambasivarao, S. V.; Acevedo, O. Development of OPLS-AA (40) Sambasivarao, S. V.; Acevedo, O. Development of OrLS-AA Force Field Parameters for 68 Unique Ionic Liquids. J. Chem. Theory Comput. 2009, 5, 1038–1050.
  (41) McDaniel, J. G.; Choi, E.; Son, C. Y.; Schmidt, J. R.; Yethiraj, A. Conformational and Dynamic Properties of
- Poly(ethylene oxide) in an Ionic Liquid: Development and Implementation of a First-Principles Force Field. J. Phys. Chem. B **2016**, 120, 231–243.
- (42) Martyna, G. J.; Tuckerman, M. E.; Tobias, D. J.; Klein, M. Explicit Reversible Integrators for Extended Systems Dynamics. Mol. Phys. 1996, 87, 1117–1157.
  (43) Towns, J.; Cockerill, T.; Dahan, M.; Foster, I.; Gaither, K.;
- Grimshaw, A.; Hazlewood, V.; Lathrop, S.; Lifka, D.; Peterson, G. D.; Roskies, R.; Scott, J. R.; Wilkins-Diehr, N. XSEDE: Accelerating Scientific Discovery. Comput. Sci. Eng. 2014, 16, 62 - 74.

## Graphical TOC Entry

